

# The $\pi$ , $K^+$ , and $K^0$ electromagnetic form factors

Pieter Maris and Peter C. Tandy  
*Center for Nuclear Research, Department of Physics,  
Kent State University, Kent OH 44242*  
(February 8, 2008)

The rainbow truncation of the quark Dyson–Schwinger equation is combined with the ladder Bethe–Salpeter equation for the meson amplitudes and the dressed quark-photon vertex in a self-consistent Poincaré-invariant study of the pion and kaon electromagnetic form factors in impulse approximation. We demonstrate explicitly that the current is conserved in this approach and that the obtained results are independent of the momentum partitioning in the Bethe–Salpeter amplitudes. With model gluon parameters previously fixed by the condensate, the pion mass and decay constant, and the kaon mass, the charge radii and spacelike form factors are found to be in good agreement with the experimental data.

Pacs Numbers: 24.85.+p, 14.40.Aq, 13.40.Gp, 11.10.St

## I. INTRODUCTION

The light pseudoscalar mesons play an important role in understanding low-energy QCD. They are the lightest observable hadronic bound states of a quark and an anti-quark, and are the Goldstone bosons associated with chiral symmetry breaking. Their static properties such as the mass and decay constants have been studied extensively [1,2]. Dynamic properties and scattering observables are much less understood theoretically, but therefore not less important to calculate within QCD. In this respect, the elastic electromagnetic form factors of the pion and kaon are very interesting: the probe is well understood, there are accurate data for  $F_\pi$  at low  $Q^2$  to confront theoretical calculations with, and the charge radii  $r_\pi^2$ ,  $r_{K^+}^2$ , and  $r_{K^0}^2$  are experimentally known. Currently, there are several experiments at JLab to determine both the pion and the kaon form factor in the range  $0.5 < Q^2 < 3 \text{ GeV}^2$  to better accuracy [3,4], which could help to discriminate between different model calculations.

To calculate these form factors, we use an approach based on the Dyson–Schwinger equations [DSEs], which form an excellent tool to study nonperturbative aspects of hadron properties in QCD [5]. The approach is consistent with quark and gluon confinement [5,6], generates dynamical chiral symmetry breaking [7], and is Poincaré invariant. It is straightforward to implement the correct one-loop renormalization group behavior of QCD [2], and obtain agreement with perturbation theory in the perturbative region. Provided that the relevant Ward identities are preserved in the truncation of the DSEs, the corresponding currents are conserved. Axial current conservation induces the Goldstone nature of the pions and

kaons [8]; electromagnetic current conservation produces the correct hadronic charge without fine-tuning.

We obtain the meson Bethe–Salpeter amplitudes [BSAs] and the quark-photon vertex as the solutions of respectively the homogeneous and inhomogeneous Bethe–Salpeter equation [BSE] in ladder truncation. The required dressed quark propagators are obtained from solutions of the quark DSE in rainbow truncation. Non-analytic effects from vector mesons are automatically taken into account, because these vector  $q\bar{q}$  bound states appear as poles in the quark-photon vertex solution [9]. We employ a realistic model for the effective quark-antiquark coupling that has been shown to reproduce the pion and kaon masses and decay constants [2] as well as the masses and decay constants for the vector mesons  $\rho$ ,  $\phi$  and  $K^*$  to within 10% [10]. The model parameters are all fixed in previous work [10] and constrained only by  $m_\pi$ ,  $m_K$ ,  $f_\pi$  and  $\langle\bar{q}q\rangle$ . The produced pion charge radius is within 2% of the experimental value [9]. Here, we use the same approach, without parameter adjustment, to calculate the neutral and charged kaon form factors and charge radii; we also extend our previous pion form factor calculations [9] to the spacelike  $Q^2$ -domain anticipated for future JLab [4] data.

In Sec. II we review the formulation that underlies a description of the pion and kaon charge form factors within a modeling of QCD through the DSEs. Within the impulse approximation, we outline the manner in which a ladder-rainbow dynamics for the propagators, BSAs and quark-photon vertex preserves the meson electromagnetic current. We further indicate the additional terms needed for current conservation, if one goes beyond rainbow-ladder truncation for the DSEs. In Sec. III we discuss the details of the model and present our numerical results for the form factors. Concluding remarks are given in Sec. IV.

## II. PSEUDOSCALAR ELECTROMAGNETIC FORM FACTORS

The 3-point function describing the coupling of a photon with momentum  $Q$  to a pseudoscalar meson with initial and final momenta  $P_\pm = P \pm Q/2$  respectively can be written as the sum of two terms

$$\Lambda_\nu^{a\bar{b}}(P, Q) = \hat{Q}^a \Lambda_\nu^{a\bar{b}a}(P, Q) + \hat{Q}^{\bar{b}} \Lambda_\nu^{a\bar{b}\bar{b}}(P, Q), \quad (1)$$

with  $\hat{Q}$  the electric charge of the (anti-)quark,  $\frac{2}{3}$  for the  $u$ -quark, and  $-\frac{1}{3}$  for the  $d$ - and  $s$ -quarks, and with  $\Lambda^{a\bar{b}a}$

and  $\Lambda^{a\bar{b}\bar{b}}$  describing the coupling of a photon to the quark and anti-quark inside the meson respectively. The meson form factor is defined as

$$\Lambda_\nu^{a\bar{b}}(P, Q) = 2 P_\nu F(Q^2), \quad (2)$$

and the corresponding charge radius as  $r^2 = -6F'(Q^2)$  at  $Q^2 = 0$ . Analogously, we can define a form factor for each of the two terms on the RHS of Eq. (1)

$$\Lambda_\nu^{a\bar{b}\bar{b}}(P, Q) = 2 P_\nu F_{a\bar{b}\bar{b}}(Q^2). \quad (3)$$

Current conservation dictates that each of the form factors  $F_{a\bar{b}\bar{b}}(Q^2)$  and  $F_{\bar{a}b\bar{a}}(Q^2)$  are 1 at  $Q^2 = 0$ .

### A. Impulse Approximation

Using dressed quark propagators, bound state BSAs, and the dressed  $q\bar{q}\gamma$ -vertex, form factors can be calculated in impulse approximation. We denote by  $\Gamma_\mu^a(q, q'; Q)$  the quark-photon vertex describing the coupling of a photon with momentum  $Q$  to a quark with final and initial momenta  $q$  and  $q' = q - Q$  respectively and flavor  $a$ . With this notation, the vertices in Eq. (1) take the form<sup>1</sup>

$$\Lambda_\nu^{a\bar{b}\bar{b}}(P, Q) = 2 N_c \int \frac{d^4 k}{(2\pi)^4} \text{Tr} \left[ S^a(q) \Gamma^{a\bar{b}}(q, q_+; P_-) \right. \\ \left. \times S^b(q_+) i\Gamma_\nu^b(q_+, q_-; Q) S^b(q_-) \bar{\Gamma}^{a\bar{b}}(q_-, q; P_+) \right], \quad (4)$$

where  $q = k + \frac{1}{2}P$ ,  $q_\pm = k - \frac{1}{2}P \pm \frac{1}{2}Q$ ,  $P_\pm = P \pm \frac{1}{2}Q$ , and analogously for  $\Lambda_\nu^{a\bar{b}\bar{a}}$ . The notation  $\int^\Lambda$  denotes a translationally-invariant regularization of the integral, with  $\Lambda$  the regularization mass-scale, which can be removed at the end of all calculations by taking the limit  $\Lambda \rightarrow \infty$ .  $S(q)$  is the dressed quark propagator and  $\Gamma^{a\bar{b}}(q, q'; P)$  is the meson BSA, with  $P^2 = -m^2$  the on-shell meson momentum, and  $q$  and  $q' = q - P$  the quark and anti-quark momenta respectively.

Both  $S(q)$  and  $\Gamma^{a\bar{b}}(q, q'; P)$  are solutions of their respective DSEs

$$S(p)^{-1} = Z_2 i \not{p} + Z_4 m(\mu) \\ + Z_1 \int \frac{d^4 q}{(2\pi)^4} g^2 D_{\mu\nu}(p - q) \frac{\lambda^i}{2} \gamma_\mu S(q) \Gamma_\nu^i(q, p), \quad (5)$$

and

$$\Gamma^{a\bar{b}}(p, p'; Q) = \int \frac{d^4 q}{(2\pi)^4} K(p, q; Q) \chi^{a\bar{b}}(q, q'; Q), \quad (6)$$

where  $D_{\mu\nu}(k)$  is the renormalized dressed-gluon propagator,  $\Gamma_\nu^i(q, p)$  is the renormalized dressed quark-gluon vertex,  $K$  is the renormalized  $\bar{q}q$  scattering kernel that is irreducible with respect to a pair of  $\bar{q}q$  lines, and  $\chi^{a\bar{b}}(q, q'; Q) = S^a(q) \Gamma^{a\bar{b}}(q, q'; Q) S^b(q')$  is the BS wave function.

The solution of Eq. (5) is renormalized according to  $S(p)^{-1} = i \not{p} + m(\mu)$  at a sufficiently large spacelike  $\mu^2$ , with  $m(\mu)$  the renormalized quark mass at the scale  $\mu$ . In Eq. (5),  $S$ ,  $\Gamma_\mu^i$  and  $m(\mu)$  depend on the quark flavor, although we have not indicated this explicitly. The renormalization constants  $Z_2$  and  $Z_4$  depend on the renormalization point and the regularization mass-scale, but not on flavor: in our analysis we employ a flavor-independent renormalization scheme.

The meson BSAs  $\Gamma^{a\bar{b}}(q, q'; P)$  are normalized according to the canonical normalization condition

$$P_\mu = N_c \frac{\partial}{\partial P_\mu} \int \frac{d^4 q}{(2\pi)^4} \left\{ \text{Tr} \left[ \bar{\Gamma}^{a\bar{b}}(\tilde{q}', \tilde{q}; Q) \right. \right. \\ \left. \left. \times S^a(q + \eta P) \Gamma^{a\bar{b}}(\tilde{q}, \tilde{q}'; Q) S^b(q + (\eta - 1)P) \right] + \right. \\ \left. \int \frac{d^4 k}{(2\pi)^4} \text{Tr} \left[ \bar{\chi}^{a\bar{b}}(\tilde{k}', \tilde{k}; Q) K(\tilde{k}, \tilde{q}; P) \chi^{a\bar{b}}(\tilde{q}, \tilde{q}'; Q) \right] \right\}, \quad (7)$$

at the mass shell  $P^2 = Q^2 = -m^2$ , with  $\tilde{q} = q + \eta Q$ ,  $\tilde{q}' = q + (\eta - 1)Q$ , and similarly for  $\tilde{k}$  and  $\tilde{k}'$ . We use the conventions where  $f_\pi = 92$  MeV, and  $\eta$  describes the momentum partitioning between the quark and anti-quark. Note that physical observables should be independent of this parameter.

For pseudoscalar bound states the BSA is commonly decomposed into [2]

$$\Gamma(k + \eta P, k + (\eta - 1)P; P) = \\ = \gamma_5 [iE(k^2; k \cdot P; \eta) + \not{P} F(k^2; k \cdot P; \eta) \\ + \not{k} G(k^2; k \cdot P; \eta) + \sigma_{\mu\nu} k_\mu P_\nu H(k^2; k \cdot P; \eta)], \quad (8)$$

with the invariant amplitudes  $E$ ,  $F$ ,  $G$  and  $H$  being Lorentz scalar functions of  $k^2$  and  $k \cdot P = kP \cos \theta$ . Subsequently, each invariant amplitude can be expanded in  $k \cdot P$  based on Chebyshev polynomials

$$f(k^2, k \cdot P; P^2) = \sum_{i=0}^{\infty} U_i(\cos \theta) (kP)^i f_i(k^2; P^2). \quad (9)$$

For charge-parity eigenstates, such as the pion, the invariant amplitudes  $E$ ,  $F$ ,  $G$ , and  $H$  have a well-defined charge-parity if one chooses  $\eta = \frac{1}{2}$ . Therefore, these amplitudes are either entirely even ( $E$ ,  $F$ , and  $H$ ) or odd ( $G$ ) in  $k \cdot P$ , and one needs only the even (or odd) Chebyshev moments to completely describe these amplitudes, which makes this a convenient decomposition.

<sup>1</sup>We use Euclidean metric  $\{\gamma_\mu, \gamma_\nu\} = 2\delta_{\mu\nu}$ ,  $\gamma_\mu^\dagger = \gamma_\mu$  and  $a \cdot b = \sum_{i=1}^4 a_i b_i$ .

## B. The quark-photon vertex

The quark-photon vertex is the solution of the renormalized inhomogeneous BSE

$$\Gamma_\mu^a(p_+, p_-; Q) = Z_2 \gamma_\mu + \int^\Lambda \frac{d^4 q}{(2\pi)^4} K(p, q; Q) \times S^a(q_+) \Gamma_\mu^a(q_+, q_-; Q) S^a(q_-), \quad (10)$$

with  $p_\pm = p \pm \frac{1}{2}Q$  and  $q_\pm = q \pm \frac{1}{2}Q$ , and with the same kernel  $K$  as the homogeneous BSE for meson bound states. Because of gauge invariance, it satisfies the Ward–Takahashi identity [WTI]

$$i Q_\mu \Gamma_\mu^a(p_+, p_-; Q) = S_a^{-1}(p_+) - S_a^{-1}(p_-). \quad (11)$$

Solutions of the homogeneous version of Eq. (10) at discrete timelike momenta  $Q^2$  define vector meson bound states with masses  $m_V^2 = -Q^2$ . It follows that  $\Gamma_\mu^a(p; Q)$  has poles at those locations, and behaves like

$$\Gamma_\mu^a(p_+, p_-; Q) \rightarrow \frac{\Gamma_\mu^{a\bar{a}V}(p_+, p_-; Q) f_V m_V}{Q^2 + m_V^2}, \quad (12)$$

in the vicinity of these bound states, where  $\Gamma_\mu^{a\bar{a}V}$  is the  $a\bar{a}$  vector meson BSA, and  $f_V$  the electroweak decay constant [10].

For the photon coupled to  $u$ - and  $d$ -quarks, this results in a  $\rho$ -meson pole at  $Q^2 = -0.6 \text{ GeV}^2$ . For the photon coupled to  $s$ -quarks, the first pole is located around  $Q^2 = -1.0 \text{ GeV}^2$  at the  $\phi$ -mass. At the level of the ladder approximation, which is commonly used in practical calculations, there is no width generated for the vector meson, and the vertex has real poles. One would have to incorporate the open  $\pi\pi$  channel in the ladder BSE kernel to produce a vector meson width; for the vertex, this would generate an imaginary part beyond the threshold for pion production,  $Q^2 < -4 m_\pi^2$  in the timelike region.

The full vertex  $\Gamma_\mu^a$  can be decomposed into 4 longitudinal components and 8 transverse components. The longitudinal components do not contribute to the form factors. In Ref. [9] it was shown that only 5 of the 8 transverse components are important for the pion form factor, in the momentum range  $-0.3 < Q^2 < 1.0 \text{ GeV}^2$  the remaining 3 components contribute less than 1%. We expect that this will also be the case for the kaon form factor, and use the Dirac amplitudes  $T_1$  to  $T_5$  of Ref. [9] only.

## C. Charge conservation

At  $Q = 0$  the quark-photon vertex is completely specified by the differential Ward identity

$$i \Gamma_\mu^b(p, p; 0) = \frac{\partial}{\partial p_\mu} S_b^{-1}(p). \quad (13)$$

If this is inserted in Eq. (4), one finds after a change of integration variables  $k \rightarrow k - \frac{1}{2}P$

$$\Lambda_\nu^{a\bar{b}}(P, 0) = 2P_\nu F_{a\bar{b}}(0) = 2N_c \int^\Lambda \frac{d^4 q}{(2\pi)^4} \text{Tr}[\bar{\Gamma}^{a\bar{b}}(q', q; P) S^a(q) \Gamma^{a\bar{b}}(q, q'; P) \frac{\partial S^b(q-P)}{\partial P}], \quad (14)$$

with  $q' = q - P$ . Comparing this expression with Eq. (7) with  $\eta = 0$ , we recognize that the physical result  $F(Q^2 = 0) = 1$  follows directly from the canonical normalization condition for  $\Gamma^{a\bar{b}}$  with a BSE kernel  $K$  independent of the meson momentum  $P$ . For the ladder truncation of the kernel, which we consider in our calculation in the next section, this is the case.

With a general momentum partitioning parameter  $\eta$ , the relation between the normalization condition and electromagnetic current conservation is not so obvious. However, using a different  $\eta$  in loop diagrams (without external quark lines) is equivalent to a shift in integration variables. For processes that are not anomalous, loop integrals are independent of a shift of integration variables, provided that such a shift is performed consistently, and that all approximations employed respect Poincaré invariance. In performing such a shift, one has to take special care of the BSAs. The vertex function  $\Gamma(q, q'; P)$ , as function of the incoming and outgoing quark momenta, does not depend on  $\eta$ ; it is only in commonly used decompositions in terms of Lorentz invariant amplitudes such as Eq. (8), where  $\eta$  becomes relevant. The amplitudes  $E$ ,  $F$ ,  $G$ , and  $H$  are scalar functions of  $k^2$  and  $k \cdot P$ , which *do* depend on the choice for  $\eta$ . Under a change of  $\eta$ , some of the different Dirac structures (e.g. the amplitudes  $F$  and  $G$ ) will mix, as will the Chebyshev moments,  $f_i$  in Eq. (9). Therefore, the results will be independent of the momentum routing in the loop integrals if and only if all Dirac amplitudes *and* their dependence on  $k \cdot P$  are properly taken into account. Previously it has been shown that under these conditions the decay constants are indeed independent of  $\eta$  [2].

Use of a bare quark-photon vertex, in combination with dressed propagators, in Eq. (4), clearly violates charge conservation and leads to  $F_\pi(0) \neq 1$ . With the Ball–Chiu Ansatz [11], which is commonly used in DSE studies of electromagnetic interactions [12–17], the electromagnetic current is explicitly conserved,  $F(Q^2 = 0) = 1$ . However, the behavior of the form factor away from  $Q^2 = 0$  is not constrained by current conservation, and in the present model, use of the Ball–Chiu Ansatz leads to a value for  $r_\pi^2$  which is about 50% too small [9]. With the quark-photon vertex as the solution of the ladder BSE, together with quark propagators from the rainbow DSE, we satisfy all constraints from current conservation, and the calculated value of  $r_\pi^2$  is within 5% of the experimental value [9].

### D. Beyond rainbow-ladder truncation

If one goes beyond the rainbow-ladder truncation for the DSEs for the propagators, BSAs and quark-photon vertex, one has to go beyond impulse approximation for the form factors in order to ensure current conservation. For example, one could include higher-order  $\alpha_s$  corrections to the rainbow-ladder DSE and BSE kernels, as depicted in Fig. 1. Following the general procedure developed in Ref. [18], one can show that both the WTI, Eq. (11), and the differential Ward identity, Eq. (13), are preserved in the truncation indicated in Fig. 1, as is the axial-vector WTI, which is important for the Goldstone nature of the pions.

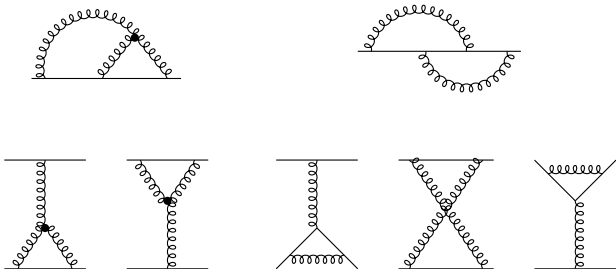


FIG. 1. The two leading-order vertex corrections to the rainbow DSE (top) and the corresponding five diagrams to be added to the ladder BSE kernel (bottom) for consistency with the relevant WTIs. The quark and gluon lines indicate dressed propagators in this and the subsequent figures.

The resulting BSE kernel  $K(q, p; P)$  now becomes dependent on the meson momentum  $P$ , which means that the second term of the normalization condition, Eq.(7), is nonzero. To be specific, with the choice  $\eta = 0$ , this introduces the four extra terms in the normalization condition, diagrammatically depicted in Fig. 2. These four additional diagrams can be generated from the BSE kernel in the bottom part of Fig. 1 by taking the derivative with respect to the meson momentum  $P$ , where  $P$  flows through one quark propagator only.

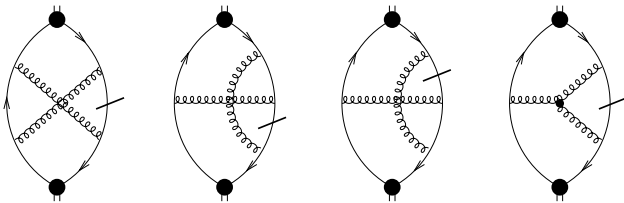


FIG. 2. The four diagrams due to the  $P$ -dependence of the kernel in the normalization condition, Eq. (7), if one includes the diagrams of Fig. 1 into the DSE dynamics, and chooses all of the meson momentum  $P$  to flow through one quark only. The derivatives with respect to  $P$  are marked by slashes.

Since taking the derivative with respect to  $P$  is equivalent to the insertion of a zero-momentum photon accord-

ing to the differential WTI, Eq. (11), it is obvious which diagrams have to be added to the impulse approximation to ensure current conservation, see Fig. (3). In the limit  $Q \rightarrow 0$  these four additional diagrams become identical to the four additional diagrams in Fig. (2), provided that the vertex satisfies the differential WTI. Of course, there are similar contributions to  $\Lambda^{aba}$ , which can be identified with terms in the normalization condition with  $\eta = 1$ .

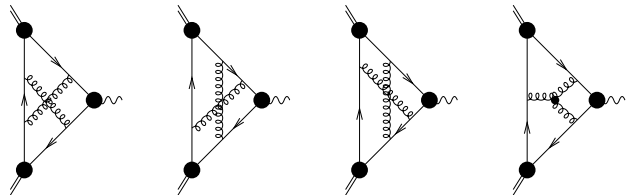


FIG. 3. The four additional contributions to the impulse approximation, Eq. (4), in order to ensure current conservation if one includes the diagrams of Fig. 1 into the DSE dynamics.

Also, simple addition of contributions due to pion and kaon loops to Eq. (4), in combination with a ladder-rainbow truncation for the DSEs, will generally violate current conservation. Current conservation requires a consistent treatment of the kernels for both the DSE and BSE equations and the approximation for the photon-hadron coupling. At present it is not clear how to incorporate meson loops self-consistently in such an approach, but we expect corrections coming from such loops to be small in the spacelike region. In Ref. [19] it was demonstrated that the quark core can generate most of the pion charge radius, and that pion loops contribute less than 15% to  $r_\pi^2$ . For larger values of  $Q^2$  the effect from meson loops reduces even further, and for  $Q^2 > 1 \text{ GeV}^2$  we expect the contribution of such loops to be negligible.

### III. MODEL CALCULATIONS

For the BSE we use a ladder truncation

$$K(p, q; P) \rightarrow -\mathcal{G}(k^2) D_{\mu\nu}^{\text{free}}(k) \frac{\lambda^a}{2} \gamma_\mu \otimes \frac{\lambda^a}{2} \gamma_\nu, \quad (15)$$

where  $D_{\mu\nu}^{\text{free}}(k = p - q)$  is the free gluon propagator in Landau gauge. The resulting BSE is consistent with a rainbow truncation  $\Gamma_v^a(q, p) \rightarrow \gamma_\nu \lambda^a / 2$  for the quark DSE, Eq. (5), in the sense that the combination produces vector and axial-vector vertices satisfying the respective WTIs. In the axial case, this ensures that in the chiral limit the ground state pseudoscalar mesons are the massless Goldstone bosons associated with chiral symmetry breaking [2,8]. In the vector case, this ensures electromagnetic current conservation.

The model is completely specified once a form is chosen for the “effective coupling”  $\mathcal{G}(k^2)$ . We employ the Ansatz [2,10]

$$\frac{\mathcal{G}(k^2)}{k^2} = \frac{4\pi^2 D k^2}{\omega^6} e^{-k^2/\omega^2} + \frac{4\pi^2 \gamma_m \mathcal{F}(k^2)}{\frac{1}{2} \ln \left[ \tau + \left( 1 + k^2/\Lambda_{\text{QCD}}^2 \right)^2 \right]}, \quad (16)$$

with  $\gamma_m = 12/(33 - 2N_f)$  and  $\mathcal{F}(s) = (1 - \exp \frac{-s}{4m_t^2})/s$ . This Ansatz preserves the one-loop renormalization group behavior of QCD, and ensures that we reproduce perturbation theory in the perturbative region. The first term of Eq. (16) implements the strong infrared enhancement in the region  $0 < k^2 < 1 \text{ GeV}^2$  which is a phenomenological requirement for sufficient dynamical chiral symmetry breaking to produce an acceptable strength for the quark condensate [20]. We use  $m_t = 0.5 \text{ GeV}$ ,  $\tau = e^2 - 1$ ,  $N_f = 4$ ,  $\Lambda_{\text{QCD}} = 0.234 \text{ GeV}$ , and a renormalization point  $\mu = 19 \text{ GeV}$ , well in the perturbative region [2,10]. The remaining parameters,  $\omega = 0.4 \text{ GeV}$  and  $D = 0.93 \text{ GeV}^2$ , are fitted to give a good description of the chiral condensate,  $m_{\pi/K}$  and  $f_{\pi}$ . The subsequent values for  $f_K$  and the masses and decay constants of the vector mesons  $\rho, \phi, K^*$  are in agreement with the experimental data [10], see Table I.

TABLE I. Overview of the results of the model for the meson masses and decay constant, adapted from Refs. [2,10]. The experimental value for the condensate is taken from Ref. [21].

|                                     | experiment [22]<br>(estimates) | calculated<br>( <sup>†</sup> fitted) |
|-------------------------------------|--------------------------------|--------------------------------------|
| $m_{\mu=1\text{GeV}}^{u=d}$         | 5 - 10 MeV                     | 5.5 MeV                              |
| $m_{\mu=1\text{GeV}}^s$             | 100 - 300 MeV                  | 125 MeV                              |
| $-\langle \bar{q}q \rangle_{\mu}^0$ | $(0.236 \text{ GeV})^3$        | $(0.241^{\dagger})^3$                |
| $m_{\pi}$                           | 0.1385 GeV                     | $0.138^{\dagger}$                    |
| $f_{\pi}$                           | 0.0924 GeV                     | $0.093^{\dagger}$                    |
| $m_K$                               | 0.496 GeV                      | $0.497^{\dagger}$                    |
| $f_K$                               | 0.113 GeV                      | 0.109                                |
| $m_{\rho}$                          | 0.770 GeV                      | 0.742                                |
| $f_{\rho}$                          | 0.216 GeV                      | 0.207                                |
| $m_{K^*}$                           | 0.892 GeV                      | 0.936                                |
| $f_{K^*}$                           | 0.225 GeV                      | 0.241                                |
| $m_{\phi}$                          | 1.020 GeV                      | 1.072                                |
| $f_{\phi}$                          | 0.236 GeV                      | 0.259                                |

## A. Results for $u\bar{u}u$ , $u\bar{s}u$ , and $u\bar{s}\bar{s}$ form factors

The pion and kaon form factors are given by

$$F_{\pi}(Q^2) = \frac{2}{3}F_{u\bar{d}u}(Q^2) + \frac{1}{3}F_{u\bar{d}\bar{d}}(Q^2), \quad (17)$$

$$F_{K^+}(Q^2) = \frac{2}{3}F_{u\bar{s}u}(Q^2) + \frac{1}{3}F_{u\bar{s}\bar{s}}(Q^2), \quad (18)$$

$$F_{K^0}(Q^2) = -\frac{1}{3}F_{d\bar{s}d}(Q^2) + \frac{1}{3}F_{d\bar{s}\bar{s}}(Q^2), \quad (19)$$

where the quark and anti-quark charges are evident. We work in the SU(2) isospin limit, where the strong interaction does not discriminate between  $u$ - and  $d$ -quarks, so for the pion we simply have  $F_{\pi}(Q^2) = F_{u\bar{u}u}(Q^2)$ . Thus there are only three independent form factors,  $F_{u\bar{u}u}(Q^2)$ ,  $F_{u\bar{s}u}(Q^2)$ , and  $F_{u\bar{s}\bar{s}}(Q^2)$ , which are shown in Fig. 4. Our estimate of the numerical error in these calculations is less than 1% for  $F_{u\bar{u}u}(Q^2)$ , and 2% for the other two form factors.

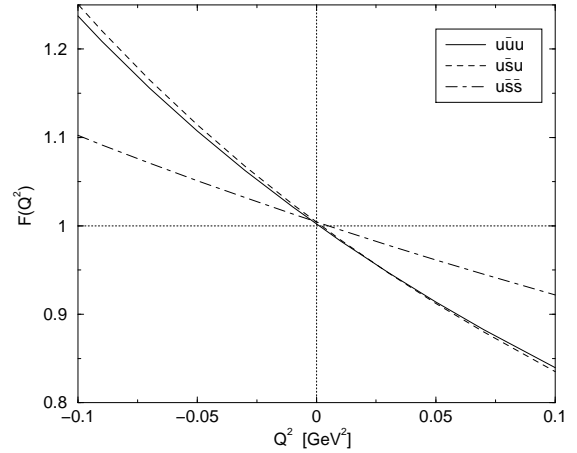


FIG. 4. The three independent form factors  $F_{u\bar{u}u}$ ,  $F_{u\bar{s}u}$  and  $F_{u\bar{s}\bar{s}}$ .

For the pion we use only the leading terms of the expansion of the BSAs and the quark-photon vertex in  $k \cdot P$ , Eq. (9). Higher order terms do not change the results more than 1% in this momentum regime, although they are needed at larger values of  $Q^2$ . For the kaon we have to use more terms in the expansion, even at  $Q^2 = 0$ , to obtain independence from the parameter  $\eta$ , and to ensure current conservation. With terms up to order  $(k \cdot P)^1$  only, there is a spread in our results of more than 10% at  $Q^2 = 0$  (from 0.94 to 1.06) if we change  $\eta$  between 0 and 1. Including the next two terms reduces that spread to less than 3%, illustrating that the result of a loop integral is independent of this unphysical parameter  $\eta$ , provided that all relevant Dirac structures and the dependence on  $k \cdot P$  are properly taken into account.

The results for  $F_{u\bar{u}u}$  and  $F_{u\bar{s}u}$  are remarkably close to each other, indicating that the flavor of the spectator quark matters very little. Within our numerical errors, they are almost indistinguishable on the  $Q^2$  domain shown. There is a slight difference in the slope of these form factors:  $r_{u\bar{u}u}^2 = 0.45 \text{ fm}^2$  versus  $r_{u\bar{s}u}^2 = 0.47 \text{ fm}^2$ . These results are in good agreement with the pion charge

radius,  $r_\pi^2 = 0.46 \text{ fm}^2$ , obtained in Ref. [9] using all eight Dirac amplitudes of the quark-photon vertex.

The result for  $F_{u\bar{s}\bar{s}}$  is quite different in that it has a significantly smaller slope characterized by a radius parameter  $r_{u\bar{s}\bar{s}}^2 = 0.21 \text{ fm}^2$ . This is due to the larger mass of the strange quark, and as a consequence the neutral kaon charge radius  $r_{K^0}^2$  will be negative. A similar effect was observed for the neutron form factor, where the heavier mass of the  $0^+(ud)$ -diquark compared to the  $d$  quark mass leads to a negative charge radius [17]. Our result is also consistent with the qualitative aspects of the vector meson dominance [VMD] picture: the lowest-mass bound state pole in the  $ss\gamma$ -vertex is the  $\phi$ , at  $Q^2 = -1.0 \text{ GeV}^2$ , which is significantly further from the photon point than is the  $\rho$  pole in the  $uu\gamma$ -vertex at  $Q^2 = -0.6 \text{ GeV}^2$ . This observation, as well as the difference between  $r_{u\bar{s}\bar{s}}^2$  and  $r_{u\bar{s}u}^2$ , is consistent with the larger mass of the strange quark.

## B. Results for the meson form factors

The results in this model for the pion form factor at low  $Q^2$ , in particular the pion charge radius, were presented previously [9]. The obtained charge radii for the kaon are presented in Table II, and are in reasonable agreement with the experimental data, without any readjustment of the model. In Fig. 5 we show our result for the charged kaon, which is in good agreement with the available data.

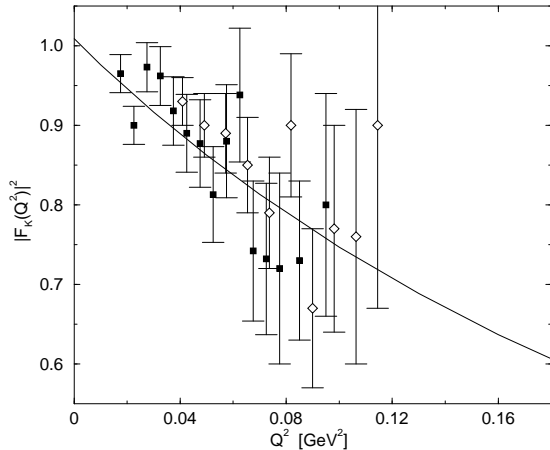


FIG. 5. The calculated  $K^+$  form factor compared to the data from Refs. [26] (open diamonds) and [24] (solid squares). Within numerical errors,  $|F_{K^+}(0)|^2 = 1$ .

TABLE II. Our results for the charge radii, compared with the experimental values given in Refs. [23–25].

| charge radii | experiment                      | calculated            |
|--------------|---------------------------------|-----------------------|
| $r_\pi^2$    | $0.44 \pm 0.01 \text{ fm}^2$    | $0.45 \text{ fm}^2$   |
| $r_{K^+}^2$  | $0.34 \pm 0.05 \text{ fm}^2$    | $0.38 \text{ fm}^2$   |
| $r_{K^0}^2$  | $-0.054 \pm 0.026 \text{ fm}^2$ | $-0.086 \text{ fm}^2$ |

Finally, in Fig. 6 we present  $Q^2 F(Q^2)$  for  $\pi$  and  $K^{0,\pm}$  for a larger  $Q^2$  range to anticipate data that may be forthcoming from experiments at JLab [3,4] and possibly other facilities in the future. In this momentum range, even for  $F_\pi(Q^2)$  the dependence on  $k \cdot P$  becomes important, and terms up to  $(k \cdot P)^3$  in Eq. (9) are required to produce a converged result at  $Q^2 = 1 \sim 3 \text{ GeV}^2$ . Higher-order terms do not change the results by more than 1% in this momentum range. Our estimate is that the net numerical accuracy for  $F_{u\bar{u}u}$ ,  $F_{u\bar{s}u}$ , and  $F_{u\bar{s}\bar{s}}$  is about 2–3% at these values of  $Q^2$ . This translates to a similar level of accuracy for  $F_\pi$  and  $F_{K^+}$ , and to a somewhat larger relative error, about 5%, for  $F_{K^0}$ , which is the difference of  $F_{u\bar{s}\bar{s}}$  and  $F_{u\bar{s}u}$ . At  $Q^2 > 3 \text{ GeV}^2$ , higher-order Chebyshev moments may be necessary, but current numerical methods prevent their accurate determination at large  $Q^2$ .

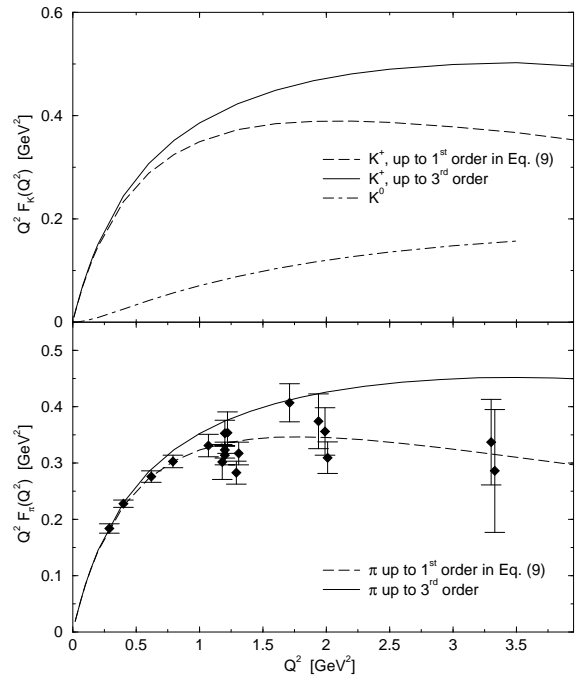


FIG. 6.  $Q^2$  times the kaon form factors (top) and pion form factor (bottom). The pion data are from Ref. [27].

Over the entire spacelike momentum range considered,  $F_\pi(Q^2) < F_{K^+}(Q^2)$ , and  $Q^2 F(Q^2)$  rises with  $Q^2$  until  $Q^2 = 3 \text{ GeV}^2$  for all three form factors. In this momentum range our results for both the pion and the  $K^+$  form factor can be fitted quite well by a simple monopole  $m^2/(Q^2 + m^2)$ , with a mass  $m^2 = 0.53 \text{ GeV}^2$  for the pion and  $m^2 = 0.61 \text{ GeV}^2$  for the  $K^+$ . A VMD model, two monopoles for the two form factors  $F_{u\bar{s}u}$  and  $F_{u\bar{s}\bar{s}}$  in Eqs. (18) and (19) with the physical  $\rho$  and  $\phi$  masses respectively, does not reproduce our results for the kaon form factors very well. For example, at  $Q^2 = 1 \text{ GeV}^2$ , VMD overshoots our  $F_{K^+}$  calculation by almost 10%, whereas the monopole fit is within 2% of our result. This difference between VMD and our calculations grows with

$Q^2$ .

Above  $Q^2 \sim 3.5 \text{ GeV}^2$  the monopole fits begin to deviate significantly from our results and  $Q^2 F(Q^2)$  starts to decrease. In a more realistic model, that takes meson loop corrections into account self-consistently, it is very well conceivable that this turn-over happens at somewhat lower values of  $Q^2$ : meson loops are expected to contribute up to 15% to  $r_\pi^2$  [19], but their contribution to the form factor decreases rapidly with increasing space-like momenta. In the presence of meson loop corrections the contribution to the form factor from the impulse approximation has to be smaller than in our calculation in order to maintain agreement with the low- $Q^2$  data. Therefore it is not unlikely that at intermediate momenta in the present approach we overestimate the form factors, which may explain the difference between the data points at  $Q^2 = 3.3 \text{ GeV}^2$  and our calculated results. More accurate results from JLab, in combination with realistic model calculations that include meson loop corrections self-consistently, may be able to resolve this question.

At asymptotically large  $Q^2$ , factorized pQCD [28] predicts that the form factor behaves like  $Q^2 F(Q^2) \rightarrow c$ , with  $c = 16\pi f_\pi^2 \alpha_s(Q^2)$ . Since our truncation and the Ansatz, Eq. (16), is constructed so as to preserve asymptotic freedom, we are guaranteed to recover the leading power-law asymptotic behavior. An explicit verification of this behavior, and calculation of the constant  $c$ , is not readily available within our present framework since numerical accuracy at large  $Q^2$  is problematic. However, it is clear from our results that at  $Q^2 \sim 4 \text{ GeV}^2$  the form factor has not yet reached its asymptotic value, and it is unlikely that experiments can access the true asymptotic region in the near future. In simplified models such as that of Ref. [15] however, it is straightforward to demonstrate that the impulse approximation does indeed lead to the power-law behavior predicted by pQCD.

#### IV. SUMMARY

We calculate the pion and kaon electromagnetic form factors within the DSE approach. The method is completely Poincaré invariant, and the only approximation made is a self-consistent truncation of the set of DSEs, which respects the relevant vector and axial-vector WTIs. The employed quark propagators, the meson BSAs, and the quark-photon vertex are solutions of their DSEs in rainbow-ladder truncation with all parameters fixed previously by fitting the chiral condensate,  $m_{\pi/K}$  and  $f_\pi$ . We include all relevant Dirac amplitudes for the BSAs and their dependence upon  $k \cdot P$ . The electromagnetic current is explicitly conserved in this approach, and there is no fine-tuning needed to obtain  $F_\pi(0) = 1 = F_{K^+}(0)$  and  $F_{K^0}(0) = 0$ . We also demonstrate explicitly that our results are (within numerical accuracy) independent of the momentum partitioning of the BSAs. The obtained pion and kaon form factors are in good agreement with

the available data over the entire  $Q^2$  range considered, and the calculated charge radii are within the error bars of their experimental values.

These charge radii are somewhat larger than those obtained in a previous study [13] that was framed in terms of semi-phenomenological representations for BSAs and confined quark propagators within the impulse approximation. The main difference with that work is that here we use numerical solutions of truncated DSEs for all the elements needed in Eq. (4), and that all our parameters were fixed previously. In comparison with theoretical calculations based on other methods, it is interesting to note that our results are very similar to those obtained in Ref. [29], in particular for the neutral kaon.

At intermediate values of  $Q^2$  our calculations are qualitatively similar to those obtained in both Ref. [13] and Ref. [29]. Up to about  $Q^2 = 3 \text{ GeV}^2$ , both  $F_\pi$  and  $F_{K^+}$  can be fitted quite well by a monopole form, with monopole masses of  $m^2 = 0.53 \text{ GeV}^2$  and  $m^2 = 0.61 \text{ GeV}^2$  respectively. At large  $Q^2$  the DSE approach does reproduce the pQCD power-law behavior [28], but this behavior does not occur until well beyond [15] the  $Q^2$  range considered in our present calculations and accessible at current accelerators.

#### ACKNOWLEDGMENTS

We acknowledge useful conversations and correspondence with C.D. Roberts, D. Jarecke and S.R. Cotanch. This work was funded by the National Science Foundation under grant No. PHY97-22429, and benefited from the resources of the National Energy Research Scientific Computing Center.

- 
- [1] see e.g. H.J. Munczek and D.W. McKay, Phys. Rev. D **39**, 888 (1989); D. Atkinson, H.J. de Groot, and P.W. Johnson, Phys. Rev. D **43**, 218 (1991); H.J. Munczek and P. Jain, Phys. Rev. D **46**, 438 (1992); M.R. Frank and C.D. Roberts, Phys. Rev. C **53**, 390 (1996).
  - [2] P. Maris and C.D. Roberts, Phys. Rev. C **56**, 3369 (1997).
  - [3] JLab experiment E93-018, spokesperson O.K. Baker.
  - [4] JLab experiment E93-021, spokesperson D. Mack.
  - [5] C.D. Roberts and S.M. Schmidt, "Density, temperature, and continuum strong coupling QCD", ANL-PHY-9530-TH-2000, and references therein.
  - [6] C.J. Burden, C.D. Roberts, and A.G. Williams, Phys. Lett. B **285**, 347 (1992); G. Krein, C.D. Roberts, and A.G. Williams, Int. J. Mod. Phys. A **7**, 5607 (1992); P. Maris, Phys. Rev. D **52**, 6087 (1995).
  - [7] see e.g. K. Higashijima, Phys. Rev. D **29**, 1228 (1984); V.A. Miransky, Phys. Lett. B **165**, 401 (1985); D. Atkinson and P.W. Johnson, Phys. Rev. D **37**, 2290 and 2296

- (1988); C.D. Roberts and B.H. McKellar, Phys. Rev. D **41**, 672 (1990).
- [8] P. Maris, C.D. Roberts and P.C. Tandy, Phys. Lett. B **420**, 267 (1998).
- [9] P. Maris and P.C. Tandy, Phys. Rev. C **61**, 045202 (2000).
- [10] P. Maris and P.C. Tandy, Phys. Rev. C **60**, 055214 (1999).
- [11] J.S. Ball and T.W. Chiu, Phys. Rev. D **22**, 2542 (1980).
- [12] C.D. Roberts, Nucl. Phys. **A605**, 475 (1996).
- [13] C.J. Burden, C.D. Roberts and M.J. Thomson, Phys. Lett. B **371**, 163 (1996).
- [14] P.C. Tandy, Prog. Part. Nucl. Phys. **39**, 117 (1997) and references therein.
- [15] P. Maris and C.D. Roberts, Phys. Rev. C **58**, 3659 (1998).
- [16] F.T. Hawes and M.A. Pichowsky, Phys. Rev. C **59**, 1743 (1999).
- [17] J.C.R. Bloch, C.D. Roberts, S.M. Schmidt, A. Bender, and M.R. Frank, Phys. Rev. C **60**, 062201 (1999).
- [18] A. Bender, C.D. Roberts, and L. von Smekal, Phys. Lett. B **380**, 7 (1996).
- [19] R. Alkofer, A. Bender, and C.D. Roberts, Int. J. Mod. Phys. **A10**, 3319 (1995).
- [20] F.T. Hawes, P. Maris, and C.D. Roberts, Phys. Lett. B **440**, 353 (1998).
- [21] D.B. Leinweber, Ann. Phys. (N.Y.) **254**, 328 (1997).
- [22] Particle Data Group, C. Caso *et al.*, Eur. Phys. J. C **3**, 1 (1998).
- [23] S.R. Amendolia *et al.*, Nucl. Phys. **B277**, 168 (1986).
- [24] S.R. Amendolia *et al.*, Phys. Lett. B **178**, 453 (1986).
- [25] W.R. Molzon *et al.*, Phys. Rev. Lett. **41**, 1213 (1978).
- [26] E.B. Dally *et al.*, Phys. Rev. Lett. **45**, 232 (1980).
- [27] C.J. Bebek *et al.*, Phys. Rev. D **16**, 1693 (1978).
- [28] G.R. Farrar and D.R. Jackson, Phys. Rev. Lett. **43**, 246 (1979); G.P. Lepage and S.J. Brodsky, Phys. Rev. D **22**, 2157 (1980).
- [29] H-M. Choi and C-R. Ji, Phys. Rev. D **59**, 074015 (1999).